Absorption and scattering perturbations in homogeneous and layered diffusive media probed by time-resolved reflectance at null source-detector separation

Lorenzo Spinelli,[1] Fabrizio Martelli,[2] Samuele Del Bianco,[3] Antonio Pifferi,[1] Alessandro Torricelli,[1] Rinaldo Cubeddu,[1] and Giovanni Zaccanti[2]

[1]*INFM-Dipartimento di Fisica and IFN-CNR, Politecnico di Milano, piazza L. da Vinci 32, I-20133 Milan, Italy*

[2]*Dipartimento di Fisica dell'Università degli Studi di Firenze, Via G. Sansone 1, I-50019 Sesto Fiorentino, Florence, Italy*

[3]*CNR-Istituto di Fisica Applicata "Nello Carrara", via Madonna del Piano 10, I-50019 Sesto Fiorentino, Florence, Italy*

(Received 25 May 2006; published 28 August 2006)

We characterize the capability of time-resolved reflectance measurements at small source-detector separation (less than 5 mm) to localize small inhomogeneities embedded in an otherwise homogeneous or layered diffusive medium. By considering both absorption and scattering inhomogeneities, we demonstrate the improvement of this approach in terms of contrast and spatial resolution, as compared to more typical set-ups involving larger source-detection separations (few centimeters). Simulations are performed exploiting an analytical perturbation approach to diffusion theory and a four-layer heterogeneous time-resolved Monte Carlo code, considering realistic tissue geometries. Exhaustive investigation in the parameters space is reported.

DOI: 10.1103/PhysRevE.74.021919 PACS number(s): 87.80.−y, 42.25.Dd, 78.20.Bh, 78.47.+p

I. INTRODUCTION

In the last decade, the possibility to investigate noninvasively biological tissues by means of red and near infrared light has more and more attracted the attention of the Biomedical Optics community [1]. Different instrumental approaches [continuous wave (CW), frequency domain and time-resolved techniques] and geometries (transmittance and reflectance) have been exploited to face several challenging and fascinating applications, such as human brain mapping, optical mammography, or arthritis detection in finger joints [2].

In particular, due to the structure of some of the tissues that can be interestingly studied with these techniques, reflectance geometry is the only possibility. In this case, one has basically an injection and collection fiber placed at a fixed distance ρ. The range of the source-detector separation is typically fixed to 20–40 mm, in order to allow the injected photons to diffuse deeply enough in the tissue [3].

The problem, when one wants to noninvasively probe biological tissues with reflectance measurements, is the sensitiveness to underlying tissue structures: how many of the collected photons carry information from such deep structures? As a matter of fact, many important biological modifications, suitable to be investigated by means of optical techniques, happen beneath several millimeters of diffusing tissue (e.g., cortex activations of the brain or tumors in the female breast). For CW measurements the depth sensitivity is accomplished by adopting large source-detector separation [4]. On the other hand, there are both theoretical and experimental evidences showing that depth sensitivity is naturally coded in the time-domain measurements, if one performs a time segmentation of the curve profiles [5–8].

Recently in a paper, we proposed a unique approach for the investigation of highly diffusive media, based on time-resolved reflectance measurements at null source-detector separation [9]. In that paper, we demonstrated by means of numerical simulations that this approach yields better spatial resolution and contrast with respect to the use of longer interfiber distances, for an absorbing pointlike inclusion embedded in a homogeneous background. Furthermore, practical implementations of this approach were suggested. Here we want to extend such results considering both absorption and scattering inclusions, also with finite dimensions. Moreover, besides the case of a simple homogeneous background, we will analyze layered geometries, better describing some biological structures, such as head or muscle, which are relevant for optical measurements. To this aim a time-resolved four-layer Monte Carlo code has been developed.

In Sec. II we describe the theoretical background, while the results of the simulations with the analysis in the parameters space are shown in Sec. III. Finally, in Sec. IV we report some conclusions.

II. THEORETICAL BACKGROUND

In a diffusive homogeneous slab the number of photons per unit area and time emerging from tissue at distance ρ from the source after having reached at least depth z is

$$N(\rho,t) = kt^{-5/2}\exp(-\mu_a v t)\exp\left(-\frac{3\mu_s'\rho^2}{4vt}\right)S(\mu_s',s_0,t)p(z,t), \tag{1}$$

where k is a constant, μ_a is the absorption coefficient, μ_s' is the reduced scattering coefficient, v is the speed of light in the medium, $S(\mu_s',s_0,t)$ is a dipole term taking into account boundary conditions and thickness s_0 of the slab, and $p(z,t)$ is the time-resolved probability that photons penetrate at a certain depth before being detected at tissue surface [6]. Since $p(z,t)$ is independent of the source-detector separation ρ and of μ_a, the ratio of photons that, at a given time, emerge at a finite source-detector separation ρ with respect to those at null separation is given by

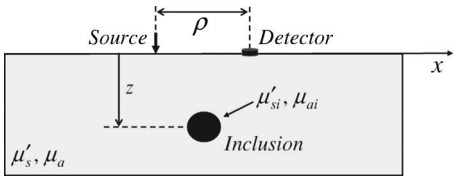

FIG. 1. Scheme of the reflectance measurement geometry in the case of an inclusion of optical properties μ'_{si}, μ_{ai} embedded in a homogeneous medium of optical properties μ'_s, μ_a.

$$G(\rho,t) = \frac{N(\rho,t)}{N(0,t)} = \exp[-(\rho/\rho_0)^2], \tag{2}$$

where we have defined $\rho_0 = \sqrt{4vt/3\mu'_s}$. For biological tissues, in the spectral range 0.6–1.0 μm, the approach at null separation distance can lead to a gain up to a 2 order of magnitude in terms of collected photons, with respect to a time-resolved reflectance measurement, where typically an interfiber distance of about 3 cm is adopted [9]. Furthermore, the new approach does not suffer from any loss of depth information because $p(z,t)$ does not depend on ρ. Furthermore, since photons received at $\rho=0$ probed a smaller volume with respect to photons at $\rho \gg 0$, we also expect to improve, in addition to the photon number, both the contrast and the localization.

III. NUMERICAL SIMULATIONS

In this section we study the features of the time-resolved reflectance measurements at null or small interfiber distances ρ, comparing the results with more classical approaches assuming $\rho \geqslant 2$ cm. To this purpose we have performed simulations exploiting an analytical perturbation model based on the diffusion theory both in a semi-infinite homogeneous medium [10] and in a layered inhomogeneous medium [11,12]. Furthermore, we have considered also a four-layer inhomogeneous medium by means of a tailored Monte Carlo code. The measurement strategies, adopting different interfiber distances, have been compared in terms of contrast and spatial resolution in the localization of an inclusion with different optical properties with respect to the background, where it is embedded.

For the homogeneous background, we considered the cases both of a more absorbing and less scattering inclusion, with different volumes (pointlike and finite-dimension inclusions). For the more absorbing inclusion, we also studied the effect exerted by changing the optical properties of the background.

Moreover, two more realistic cases have been investigated, where an absorbing inclusion is embedded in a three- or four-layer background. Finally, the case of constant or different refractive index between the layers of a bilayer medium has been considered.

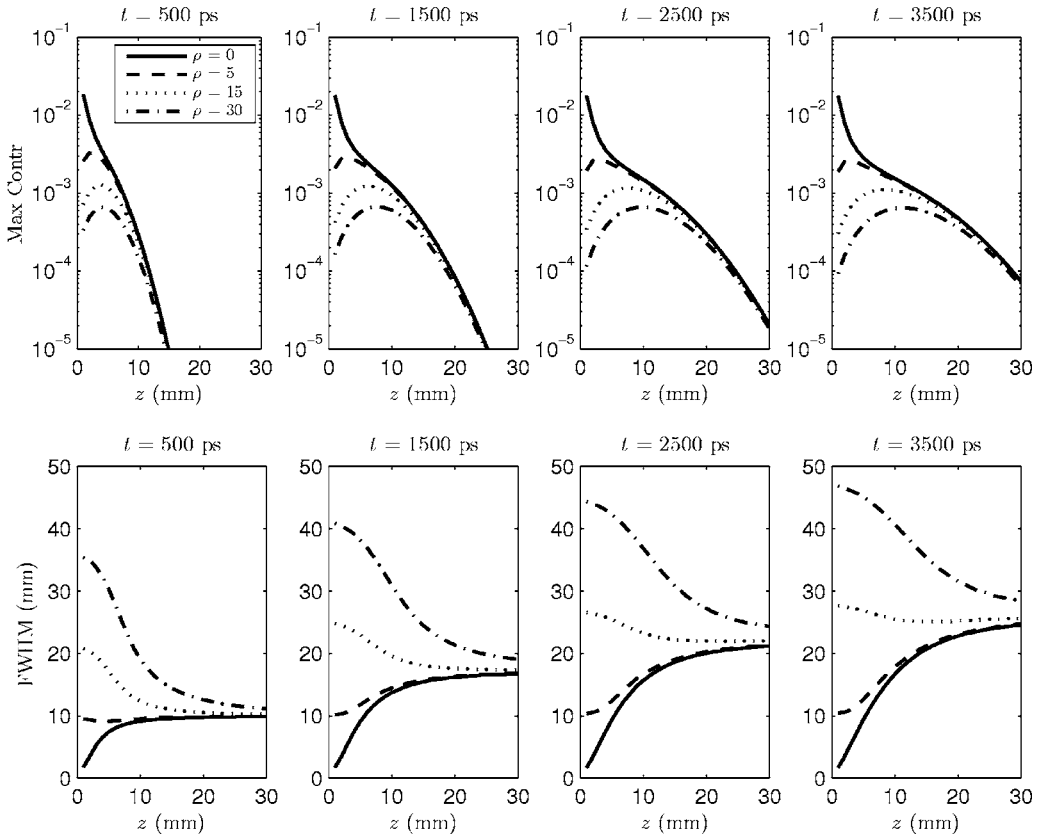

FIG. 2. Maximum (upper row) and FWHM (lower row) of the contrast line scans as a function of the inclusion depth z, for different interfiber distances ρ and times t in the case of a pointlike absorption inclusion embedded in a homogeneous medium. Optical parameters are: $\mu'_s = 1$ mm^{-1}, $\mu_a = 0.005$ mm^{-1} for background and $\mu'_{si} = 1$ mm^{-1}, $\mu_{ai} = 0.02$ mm^{-1} for the inclusion.

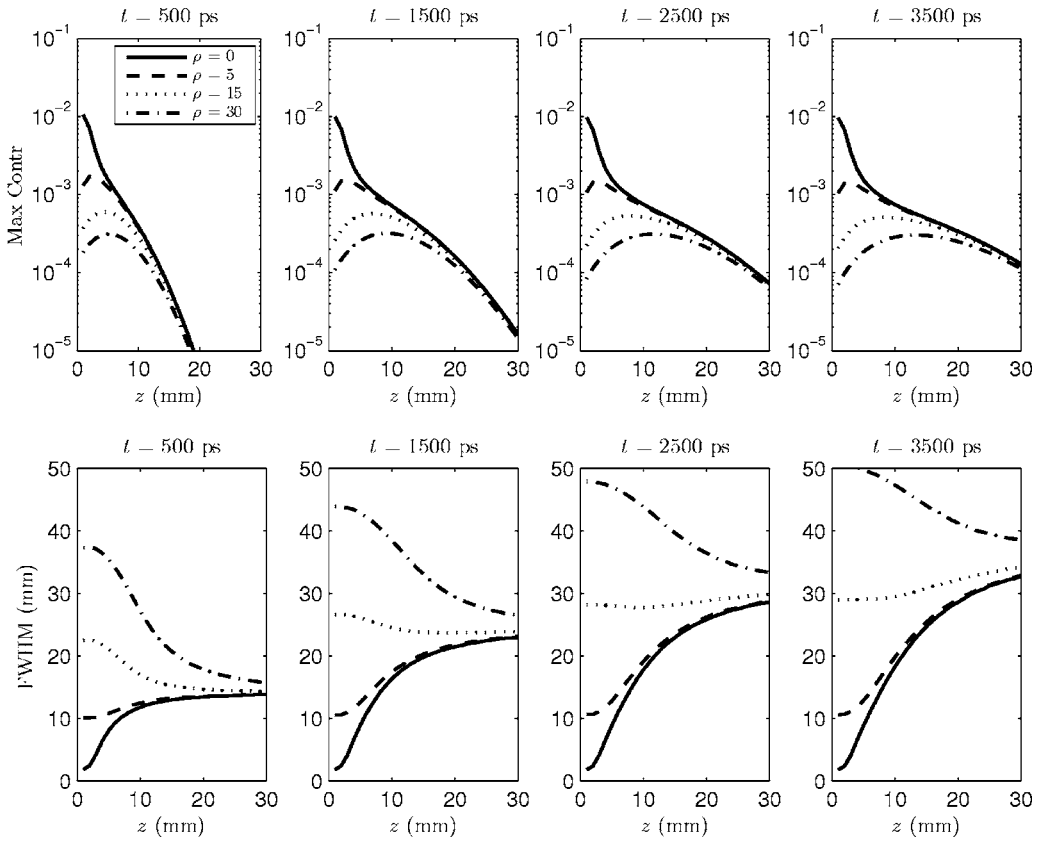

FIG. 3. The same as Fig. 1, with a less scattering background. Optical parameters are: $\mu_s'=0.5$ mm^{-1}, $\mu_a=0.005$ mm^{-1} for background and $\mu_{si}'=0.5$ mm^{-1}, $\mu_{ai}=0.02$ mm^{-1} for the inclusion.

A. The homogeneous background

First, we considered as a background a semi-infinite homogeneous medium with optical properties typical of biological tissues: reduced scattering coefficient $\mu_s'=1$ mm^{-1} and absorption coefficient $\mu_a=0.005$ mm^{-1}. A pointlike absorption inclusion (volume of 1 mm^3) has been assumed, with the following optical properties: $\mu_{si}'=1$ mm^{-1} and $\mu_{ai}=0.02$ mm^{-1}. At each depth z, time-resolved reflectance curves were calculated for different positions of the inclusion along the direction x parallel to the surface (see Fig. 1). The origin of the x axis was located at half between the source and the detector. From such line scans, the contrast

$$C(x,z;\rho,t)=\frac{N_0(\rho,t)-N(x,z;\rho,t)}{N_0(\rho,t)}, \tag{3}$$

where $N_0(\rho,t)$ and $N(x,z;\rho,t)$ are the photon counts for the homogeneous and for the inhomogeneous medium, respectively, was calculated at different times t after the injection of the pulse.

Figure 2 reports the contrast maximum and the full width at half maximum (FWHM) of the contrast line scans [see Eq. (3)], as a function of the depth z, for different interfiber distances ρ and times. As for the contrast maximum, we can see that it is higher for small ρ, at any time and depth. Furthermore, for depths larger than 10 mm, interfiber distances up to 5 mm are quite equivalent, at any time. For ρ equal or greater than 5 mm, we observe that, by moving towards later times, the contrast reaches its maximum for larger inclusion depths, by preserving its value. As for the spatial resolution, the best performances are obtained at $\rho=0$. For $\rho=0$ we can note also that the spatial resolution is quite unchanged at any time if the depth of the inclusion is less than 5 mm. Furthermore, for small interfiber distances, the spatial resolution worsens for increasing depths of the inclusion. This is due to the increasing of the volume visited by photons for reaching deeper inclusions. On the contrary, for interfiber distances larger than 15 mm, it seems that the FWHM decreases for increasing inclusion depth. This behavior is due to the "banana shape" of the photon path in the diffusing medium: for inclusion close to the surface this implies that there are two symmetric positions in the line scan where the contrast reaches its maximum value: one below the source and another below the collection position [9]. In this situation the FWHM is larger than ρ and we have the minimum information on the inclusion location. Finally, as we noted for the contrast maximum, also for inclusion depths larger than 10 mm, interfiber distances up to 5 mm are quite equivalent, at any time, in terms of spatial resolution.

Then, we considered the effects due to a larger absorbing inclusion. For this purpose an inclusion of 1000 mm^3 (a cube with a size of 10 mm) was simulated, embedded in a homogeneous medium with the same optical properties than before. For this larger inclusion, we have kept the product of volume and the absorption increment the same as the pointlike case, in order to have comparable values of the contrast.

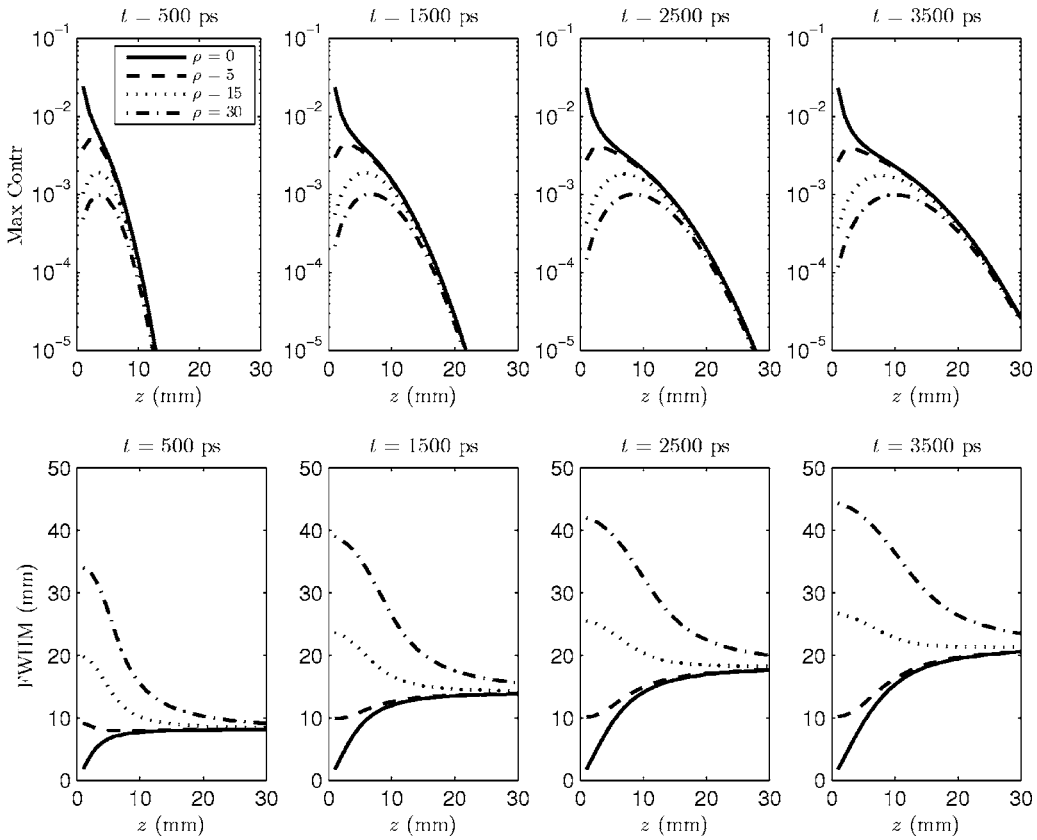

FIG. 4. The same as Fig. 1, with a more scattering background. Optical parameters are: $\mu_s'=1.5$ mm^{-1}, $\mu_a=0.005$ mm^{-1} for background and $\mu_{si}'=1.5$ mm^{-1}, $\mu_{ai}=0.02$ mm^{-1} for the inclusion.

Also for the larger inclusion, the best performances in terms of contrast and spatial resolution are obtained for null interfiber distance (data not shown). Furthermore, interfiber distances up to 5 mm gives practically the same results. Obviously this is due to the size of the inclusion. As a general comment, we can observe that considering an extended inclusion does not alter appreciably the results obtained for a pointlike inclusion.

Next, we checked the measurement approach at small interfiber distances when the optical properties of the background are changed. As for the variation of the background absorption, we note that, in the perturbation regime we are considering, all the terms in Eq. (3) contain the absorption coefficient of the background in the same multiplying exponential factor [see Eq. (2)]. Then, if we keep the same absorption increment between inclusion and background, the contrast given by Eq. (3) is independent from the value of the background absorption coefficient. So, the results presented in Fig. 2 can be considered valid for different values of the background absorption coefficient.

Then, we have varied the scattering properties of the background. First, we assumed a less scattering background and inclusion, by setting both the scattering coefficients as $\mu_s'=\mu_{si}'=0.5$ mm^{-1}. The absorption properties are the same as in Fig. 2 ($\mu_a=0.005$ mm^{-1}, $\mu_{ai}=0.02$ mm^{-1}). Next, we considered a more scattering medium, by assuming $\mu_s'=\mu_{si}'=1.5$ mm^{-1}. As before, Figs. 3 and 4 report the contrast maximum and FWHM, as a function of the depth z, for different interfiber distances ρ and times t, for a pointlike inclusion, for the less scattering and the more scattering case, respectively. By comparing Figs. 3 and 4 with Fig. 2, the trends of the contrast and the spatial resolution are the same: best performances are obtained at $\rho=0$, for any depth and time. The FWHM is increased in the case of a less scattering background and reduced otherwise. This behavior can be explained by considering that the wavelength of the photon density waves is inversely proportional to the scattering coefficient or the width of the banana shape reduces with higher μ_s' [3].

We have then considered the effects exerted by a less scattering inclusion. The study of inclusions with different scattering properties with respect to the background has important applications in optical mammography, where cysts present such a behavior [13], and in the functional study of the human brain, where activation of an area seems to be preceded by a fast variation of the scattering properties of the same area [14]. We have considered a pointlike less scattering inclusion, with the following optical properties: $\mu_{si}'=0.5$ mm^{-1} and $\mu_{ai}=0.005$ mm^{-1}, embedded in a homogeneous medium with the same properties as in Fig. 2 ($\mu_s'=1$ mm^{-1}, $\mu_a=0.005$ mm^{-1}). As we made for the absorption inclusion, we calculated the contrast reported in Eq. (3) from the time-resolved reflectance curves obtained for different depths of the inclusion and different interfiber distances. Figure 5 reports the line scans of the contrast C as a function of the position x, for different interfiber distance ρ, at various times t and depths z. In general we can see that the contrast profiles change sign, presenting some ripples. This makes it

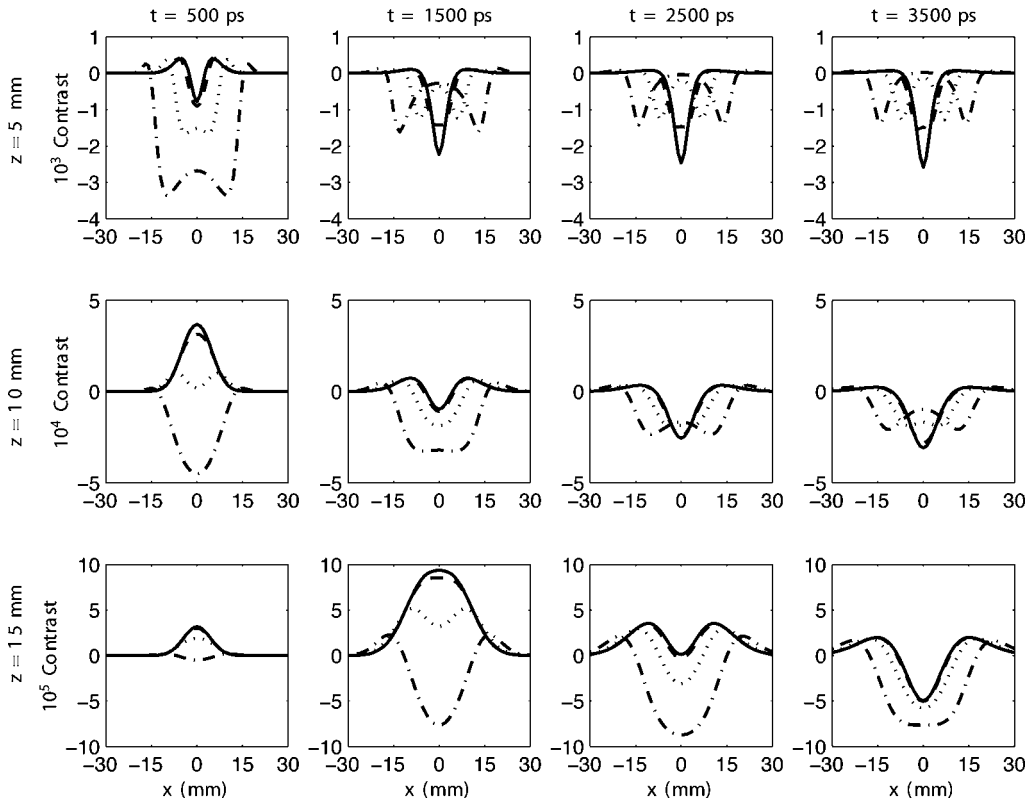

FIG. 5. Line scans of the contrast along the x axis, for different interfiber distance ρ, at various times t (different columns) and depths z (different rows), for pointlike less scattering inclusion embedded in a homogeneous medium. Optical parameters are: $\mu_s'=1$ mm^{-1}, $\mu_a=0.005$ mm^{-1} for background and $\mu_{si}'=0.5$ mm^{-1}, $\mu_{ai}=0.005$ mm^{-1} for the inclusion. In subplots, solid lines correspond to the case $\rho=0$, dashed lines to $\rho=5$ mm, dotted lines to $\rho=15$ mm and dashed-dotted lines to $\rho=30$ mm.

difficult to define a value for the maximum contrast and a FWHM of the profiles. However, for any time and depth, the features for the cases $\rho=0$ and $\rho=5$ mm are quite the same (compare solid and dashed lines in the subplots). Furthermore, for inclusion depths reported in Fig. 5, one has to increase the time in order to obtain a contrast in the case $\rho=0$ comparable to that obtained for $\rho=15$ mm or $\rho=30$ mm: for $z=5$ mm one has to consider $t\cong 1500$ ps or greater, for $z=10$ mm $t\cong 2500$ ps and for $z=15$ mm $t\cong 3500$ ps. In any case, however, the width of the profiles for $\rho=0$ or $\rho=5$ mm are definitely smaller with respect to the cases $\rho=15$ mm and $\rho=30$ mm.

From the properties of the perturbation model adopted here [10], we can infer what happens in the case of a more scattering inclusion: being the contrast proportional to the increment of the diffusion coefficient, which is inversely proportional to the scattering $[D=(3\mu_s')^{-1}]$, the plots reported in Fig. 5 are simply scaled and reversed in sign in the case of a more scattering inclusion, so the same considerations as before can be made. Furthermore, we have tested the case of a nonpointlike scattering inclusion (volume of 1 cm^3). As in the case of an absorbing inclusion, the product of volume and scattering variation has been kept the same as in the pointlike case. We observed that an increasing of the inclusion volume does not alter appreciably the results obtained for a pointlike inclusion (data not shown).

B. The layered background

We have demonstrated the advantages in terms of contrast and spatial resolution of the reflectance measurements at small interfiber distances in the simple case of homogeneous background, when the localization of an absorbing or scattering inclusion is dealt. However, a homogeneous medium is a rough approximation, especially for biological tissues. Therefore, we have complicated the geometry of the medium by considering a three-layer structure as shown in Fig. 6. Thickness of the layers were $s_1=8$ mm, $s_2=4$ mm, and $s_3=100$ mm, while optical properties were $\mu_{s1}'=1.5$ mm^{-1}, $\mu_{a1}=0.01$ mm^{-1}, $\mu_{s2}'=0.5$ mm^{-1}, $\mu_{a2}=0.005$ mm^{-1}, and $\mu_{s3}'=2.5$ mm^{-1}, $\mu_{a3}=0.005$ mm^{-1}. Simulations have been performed exploiting an analytical perturbation model based on

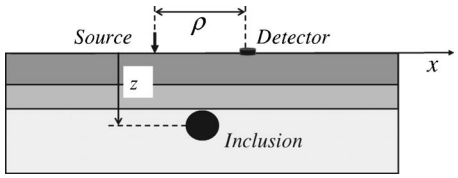

FIG. 6. Scheme for the three-layer medium ($s_1=8$ mm, $\mu_{a1}=0.01$ mm^{-1}, $\mu_{s1}'=1.5$ mm^{-1}; $s_2=4$ mm, $\mu_{a2}=0.005$ mm^{-1}, $\mu_{s2}'=0.5$ mm^{-1}; $s_3=100$ mm, $\mu_{a3}=0.005$ mm^{-1}, $\mu_{s3}'=2.5$ mm^{-1}) with an inclusion in the third layer (depth $z_i=15$ mm, volume 1 mm^3, $\mu_{si}'=1$ mm^{-1}, $\mu_{ai}=0.02$ mm^{-1}).

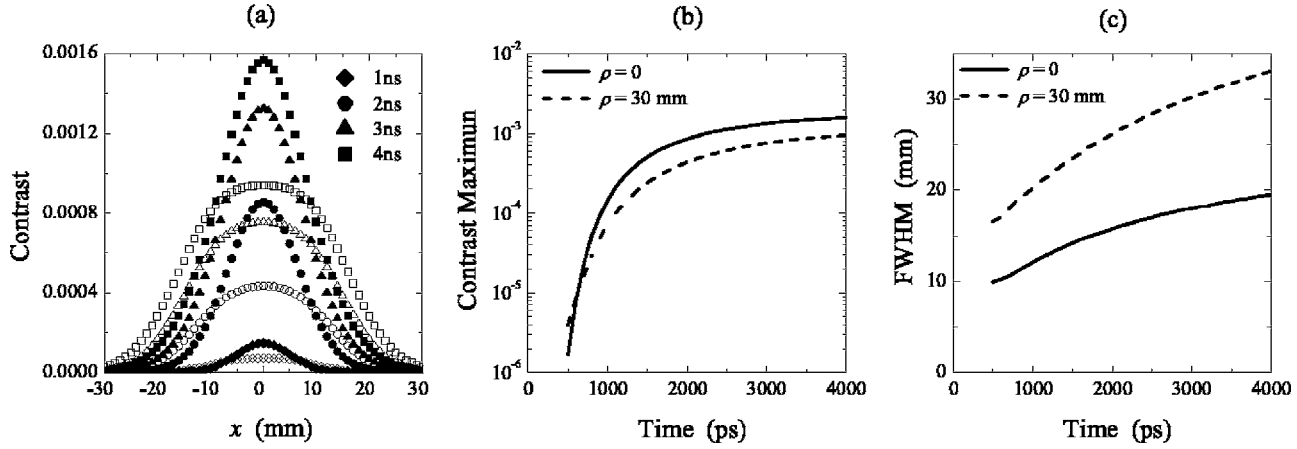

FIG. 7. (a) Scan of the contrast along the x axis at the interfiber distances $\rho=0$ (closed symbols) and $\rho=30$ mm (open symbols), for $z_i=15$ mm and times 1, 2, 3, and 4 ns, in the case of the three-layer medium. Maximum (b) and FWHM (c) of the contrast line scans as a function of time for $z_i=15$ mm. Optical parameters are the same as in Fig. 5.

the diffusion theory [11]. From Fig. 7, we can see that the results obtained in the homogeneous model are here confirmed both qualitatively and quantitatively. The approach at $\rho=0$ yields better contrast and spatial resolution.

To compare measurement approaches at $\rho=0$ and $\rho=30$ mm in an even more realistic geometry we have chosen the skin/skull, cerebrospinal fluid (CSF), white matter and gray matter combination in an adult head to mimic the scenario of a functional imaging experiment performed by time-resolved reflectance. Thickness and optical properties of the layers were chosen accordingly to Kawaguchi *et al.* [15]: $s_1=10$ mm, $\mu'_{s1}=1.70$ mm^{-1}, $\mu_{a1}=0.017$ mm^{-1}, $s_2=2$ mm, $\mu'_{s2}=0.24$ mm^{-1}, $\mu_{a2}=0.004$ mm^{-1}, $s_3=4$ mm, $\mu'_{s3}=2.20$ mm^{-1}, $\mu_{a3}=0.036$ mm^{-1}, and $s_4=1000$ mm, $\mu'_{s4}=9.10$ mm^{-1}, $\mu_{a4}=0.014$ mm^{-1}. Since an analytical diffusion approach is not suited due to the very low scattering properties of the CSF, we developed a Monte Carlo code for a four-layer inhomogeneous medium. Due to the time needed for running the Monte Carlo code (about one week to receive 2×10^5 photons if a Pentium IV, 3.2 GHz based personal computer is used), we decided not to simulate all the line scans like before, but to perform simulations in the best case for the two approaches. At $\rho=0$ this corresponds to put the source and detector coaxial with the inclusion, while for $\rho=30$ mm we located the inclusion in the middle of the source and detector fibers. For simulations we considered a receiver with a radius of 1.5 mm at $\rho=0$, and 2.6 mm at $\rho=30$ mm. Time profiles of the remitted photons are shown in Fig. 8(a) for the two approaches. It is easily observed that the increase in the source detector separation causes an overall signal attenuation and a delay due to a longer path between optodes. On the other hand, the asymptotic slope does not change since it mainly depends on the absorption coefficients in the different layers. Figure 8(b) shows the contrast due a cylindrical inhomogeneity (radius=2 mm, height=4 mm) placed in layer 3 ($z\approx14$ mm) with optical properties $\mu'_{si}=2.2$ mm^{-1}, $\mu_{ai}=0.04$ mm^{-1}, corresponding to a relative absorption contrast of 11.1% and no contrast in scattering. While at short time ($t<1$ ns) the two approaches gives comparable results, the measurements at $\rho=0$ yields higher contrast at longer time.

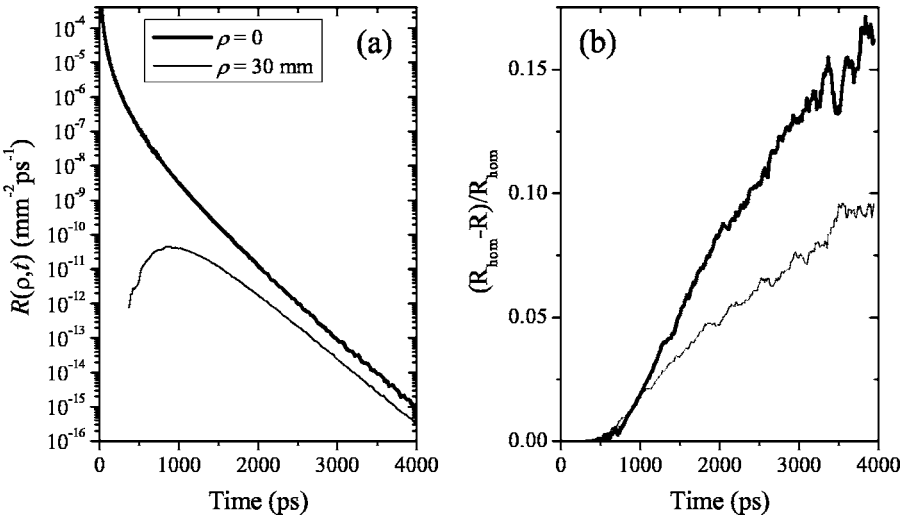

FIG. 8. (a) Time-resolved reflectance curve for interfiber distance $\rho=0$ and $\rho=30$ mm in a four-layer medium. (b) Maximum contrast as a function of time for the two approaches.

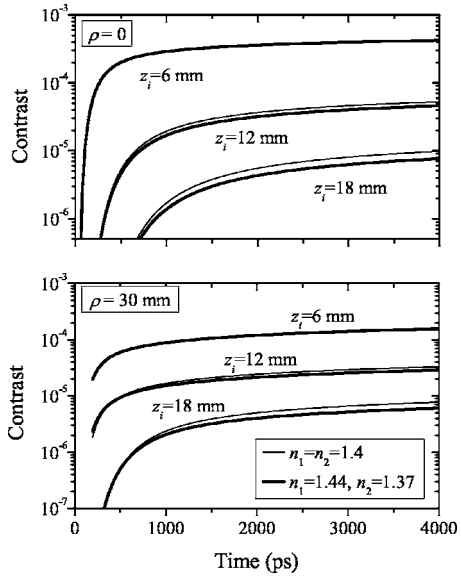

FIG. 9. Effect of the refractive index mismatch on the contrast for the two approaches ($\rho=0$ and $\rho=30$ mm). The contrast is reported as a function of time for a two-layer medium ($s_1=8$ mm, $\mu'_{s1}=1$ mm^{-1}, $\mu_{a1}=0.004$ mm^{-1}, $s_2=100$ mm, $\mu'_{s2}=0.5$ mm^{-1}, $\mu_{a2}=0.03$ mm^{-1}) both for $n_1=1.44$, $n_2=1.37$, and for $n_1=n_2=1.40$.

All the results we presented refer to media with constant refractive index. However, different types of tissue often have different refractive index n. Due both to internal reflections at the boundaries and to the different speed of light in each layer, the refractive index mismatch may significantly affect the contrast especially for small source detector separations. Since the solver we used [12] for the diffusion equation also takes into account the refractive index mismatch between the layers, we studied this point considering a two-layer medium with optical properties representative of the muscle with the subcutaneous fat layer at near infrared wavelengths. We assumed $s_1=8$ mm, $\mu'_{s1}=1$ mm^{-1}, $\mu_{a1}=0.004$ mm^{-1}, $n_1=1.44$ for the fat layer, and $s_2=100$ mm, $\mu'_{s2}=0.5$ mm^{-1}, $\mu_{a2}=0.03$ mm^{-1}, $n_2=1.37$ for muscle. As for. Fig. 8 we calculated the contrast for a pointlike absorption inclusion (volume 1 mm^3, $\Delta\mu_a=0.002$ mm^{-1}) in the best cases for the two approaches: the inclusion was coaxial with the source and detector at $\rho=0$ and in the middle of source and detector fibers at $\rho=30$ mm. The calculation was repeated for three depths: $z=6$, 12, and 18 mm. The results are shown in Fig. 9. The figure also reports the results for a medium having the same absorption and scattering properties but $n_1=n_2=1.40$. The results show that the refractive index mismatch appreciably affects the contrast only when the inclusion is in the second layer (for $z=6$ mm the curves corresponding to $n_1=n_2$ and to $n_1\neq n_2$ are indistinguishable). However, relative variations are very similar at $\rho=0$ and $\rho=30$ mm. Therefore, the results obtained for layered media with constant refractive index are also applicable when a refractive index mismatch is present.

IV. CONCLUSIONS

In this paper we studied the characteristics of time-resolved reflectance measurements in diffusive media, when interfiber distance is changed from a few millimeters to more typical values of some centimeters, in terms of contrast and spatial resolution in the localization of either an absorbing or a scattering inclusion. To this aim, numerical simulations have been performed exploiting both an analytical models and a time-resolved Monte Carlo code. Moreover, different background geometries, that is homogeneous and layered, have been considered. In the case of a homogeneous background, an extensive analysis in the parameter space has been performed, varying the optical properties of the background and also considering finite-dimension inclusions. As for the absorbing pointlike inclusion embedded in a homogeneous background, we have demonstrated that measurements at null interfiber distance give the best performances in terms of contrast and spatial resolution at any depth of the inclusion and for any time after the pulse injection. As for the scattering pointlike inclusion, the contrast in the case $\rho=0$ becomes comparable to that obtained for larger interfiber distances only if one considers times far enough from the pulse injection. Obviously, these times increase with the increasing of the inclusion depth. On the other hand, however, the width of the profiles obtained at null interfiber distance are definitely smaller with respect to the cases with larger values of ρ, demonstrating the better spatial resolution in the former case, also for the scattering inclusion. Then, for both kind of inclusions, these results are confirmed when an inclusion with finite dimensions is considered.

Then, we have also taken into account more realistic geometries of the background medium by considering different layered structures, with constant or different refractive index among the layers. In these cases, we have demonstrated that the results obtained for the homogeneous background are confirmed both qualitatively and quantitatively.

As a major point, we have demonstrated that, in general, the features of measurements performed with interfiber distances ρ from 0 to 5 mm are quite the same. This fact is very important because one can exploit more easily the advantages in terms of contrast and spatial resolution evidenced for such a kind of approach for time-resolved reflectance measurements also with ρ of the order of 5 mm, which is much less challenging from the experimental viewpoint. As a matter of fact, practical implementations of time-resolved reflectance measurements at small interfiber distances is made difficult by the presence of the early photons: as an example, with reference to Fig. 8, we have calculated that the percentage fraction of photons detected in the first 750 ps is 99.995%, 99.94%, and 99.58% for $\rho=0$, 3 and 6 mm, respectively, while it is 19.5% for $\rho=30$ mm. However, also the number of useful (i.e., late) photons increases, when interfiber distance is reduced. Then, when one works at small ρ, one must reject early photons, in order to avoid that they blind his detection system. The fact that one can set $\rho=5$ mm with no significant losses in terms of contrast and spatial resolution with respect to $\rho=0$, is of great advantage: the rejection factor of the early photons, in fact, can be reduced to less than 3 orders of magnitude in this case [9].

In the paper [9], various experimental possibilities have been proposed in order to perform time-resolved reflectance measurements at small interfiber distances, facing the problem of early photon rejection. One of the more promising

seems to be the use of a single-photon avalanche diode (SPAD) [16] as a detector operated in a time-gated mode. Following this idea, we have assembled an experimental setup, with the detection stage based on a SPAD, synchronized by a delay generator, in order to switch on the diode only after the burst of the early photons, and on a time-correlated single-photon counting system. In this way preliminary time-resolved reflectance measurements at $\rho = 2$ mm have been obtained, demonstrating efficient rejection of early photons without distortion of the tail of the photon time distribution [17]. Work is in progress to test this unique technique both on phantoms and *in vivo* for biomedical applications.

ACKNOWLEDGMENTS

This work was partially supported by MIUR under the project PRIN2005 (prot. 2005025333).

[1] A. Yodh and B. Chance, Phys. Today **48**, 34 (1995).
[2] For recent results see *Biomedical Optics 2006 Technical Digest* (Optical Society of America, Washington, DC, 2006).
[3] S. Feng, F. Zeng, and B. Chance, Appl. Opt. **34**, 3826 (1995).
[4] G. H. Weiss, Appl. Opt. **37**, 3558 (1998).
[5] J. Steinbrink, H. Wabnitz, H. Obrig, A. Villringer, and H. Rinneberg, Phys. Med. Biol. **46**, 879 (2001).
[6] S. Del Bianco, F. Martelli, and G. Zaccanti, Phys. Med. Biol. **47**, 4131 (2002).
[7] J. J. Selb, J. J. Stott, M. A. Franceschini, A. G. Sorensen, and D. A. Boas, J. Biomed. Opt. **10**, 011013 (2005).
[8] C. Sato, M. Shimada, Y. Hoshi, and Y. Yamada, J. Biomed. Opt. **10**, 064008 (2005).
[9] A. Torricelli, A. Pifferi, L. Spinelli, R. Cubeddu, F. Martelli, S. Del Bianco, and G. Zaccanti, Phys. Rev. Lett. **95**, 078101 (2005).
[10] S. Carraresi, T. S. M. Shatir, F. Martelli, and G. Zaccanti, Appl. Opt. **40**, 4622 (2001).
[11] F. Martelli, S. Del Bianco, and G. Zaccanti, Phys. Med. Biol. **50**, 2159 (2005).
[12] F. Martelli, S. Del Bianco, and G. Zaccanti, Phys. Rev. E **70**, 011907 (2004).
[13] P. Taroni, G. M. Danesini, A. Torricelli, A. Pifferi, L. Spinelli, and R. Cubeddu, J. Biomed. Opt. **9**, 464 (2004).
[14] J. Steinbrink, F. C. D. Kempf, A. Villringer, and H. Obrig, Neuroimage **26**, 996 (2005).
[15] H. Kawaguchi, T. Hayashi, T. Kato, and E. Okada, Phys. Med. Biol. **49**, 2753 (2004).
[16] S. Cova, M. Ghioni, A. Lacaita, C. Samori, and F. Zappa, Appl. Opt. **35**, 1956 (1996).
[17] A. Pifferi, A. Torricelli, L. Spinelli, R. Cubeddu, F. Martelli, G. Zaccanti, S. Del Bianco, A. Tosi, F. Zappa, and S. Cova, "Time-resolved diffuse reflectance at null source-detector separation: a novel approach to photon migration," in *Biomedical Optics 2006 Technical Digest* (Optical Society of America, Washington, DC, 2006), TuD5.